



1 **Implementation of the ORACLE (v1.0) organic
2 aerosol composition and evolution module into the
3 EC-Earth3-AerChem model**

4

5

6 Stylianos Kakavas¹, Stelios Myriokefalitakis², Alexandra P. Tsimpidi³, Vlassis A.
7 Karydis³, and Spyros N. Pandis^{1,4}

8 ¹Institute of Chemical Engineering Sciences, Foundation for Research and
9 Technology Hellas, Patras, Greece

10 ²Institute for Environmental Research and Sustainable Development (IERSD),
11 National Observatory of Athens, Penteli, Greece

12 ³Institute for Energy and Climate Research, IEK-8 Troposphere, Forschungszentrum
13 Jülich GmbH, Jülich, Germany

14 ⁴Department of Chemical Engineering, University of Patras, Patras, Greece
15

16 *Correspondence to:* Spyros N. Pandis (spyros@chemeng.upatras.gr) and Stelios
17 Myriokefalitakis (steliosm@noa.gr).

18

19 **Abstract.** Simulating the composition and evolution of organic aerosol (OA) in Earth
20 System Models (ESMs) presents significant challenges due to the high computational
21 demands of detailed chemical mechanisms. The computationally efficient ORACLE
22 module employs the volatility basis set framework and can simulate secondary
23 organic aerosol (SOA) formation from a range of precursors, including volatile
24 (VOCs), intermediate-volatility (IVOCs), semi-volatile (SVOCs), and low-volatility
25 organic compounds (LVOCs). In this study, a lite configuration of the ORACLE v1.0
26 module (ORACLE-lite) is implemented into the TM5-MP global chemical transport
27 model (CTM), which represents the chemistry-transport component of the EC-Earth3-
28 AerChem ESM. SOA formation from anthropogenic VOCs is neglected to reduce the
29 number of surrogate species and further improve computational efficiency. For the
30 standalone TM5-MP simulation, the global annual mean surface total OA
31 concentration using ORACLE-lite is approximately $1.1 \mu\text{g m}^{-3}$, representing a 25%
32 increase compared to the previous version of the model. The annual atmospheric OA
33 burden also increases by 50%, reaching 3.67 Tg. Corresponding predictions from EC-
34 Earth3-AerChem are slightly higher, with a surface total OA concentration of $1.16 \mu\text{g m}^{-3}$
35 and an atmospheric burden of 3.83 Tg, representing increases of 30% and



36 60%, respectively, compared to the previous version of the model. Comparison of
37 monthly measured PM_{2.5} OA concentrations from Europe and the US with the
38 corresponding predictions shows that the models bias is reduced by approximately
39 half in the standalone TM5-MP simulation and by a factor of three in EC-Earth3-
40 AerChem when ORACLE-lite is implemented. These enhancements enable more
41 accurate and computationally feasible assessments of the climate impacts of
42 individual organic aerosol components in future ESM studies.

43

44 **1. Introduction**

45 Atmospheric particulate matter (PM) not only affects air quality and human health but
46 also has significant implications for the climate (Monks et al., 2009; Shrivastava et
47 al., 2017; Zhang et al., 2020). Organic aerosol (OA) is a major component of PM
48 contributing between 20% and 90% to the total aerosol mass (Kanakidou et al., 2005;
49 Zhang et al., 2007; Tsipidou et al., 2025). Since anthropogenic carbonaceous
50 emissions are significant contributors to climate forcing and air pollution (IPCC,
51 2021), it is important to simulate the chemical composition and evolution of OA in
52 Earth System Models (ESMs). This will reduce uncertainties related to aerosols and
53 improve climate predictions.

54 Organic mass is categorized into primary (POA) and secondary organic
55 aerosol (SOA) based on its formation mechanism. Particulate organic mass that is
56 directly emitted into the atmosphere from various sources is referred to as POA. In
57 contrast, SOA is produced in the atmosphere through the oxidation of gas-phase
58 organic compounds. SOA is often the dominant component of OA (Zhang et al.,
59 2007; Crippa et al., 2013; Hu et al., 2016; Nault et al., 2018). However, SOA
60 concentrations are often underestimated in global climate and chemical transport
61 models (Heald et al., 2005; Tsigaridis et al., 2014; Tsipidou et al., 2016; Bergman et
62 al., 2022). This is partially due to neglected processes in the models (Robinson et al.,
63 2007), such as the evaporation of POA, the oxidation of the resulting vapors in the gas
64 phase and their subsequent condensation into the particle phase, SOA formation from
65 intermediate-volatility organic compounds (IVOCs) and the chemical aging of
66 volatile organic compounds (VOCs). Many studies have shown that the
67 photooxidation of emissions from fossil fuel combustion and biomass burning can
68 lead to the formation of significant SOA concentrations (Kroll and Seinfeld, 2008;



69 Grieshop et al., 2009; Hennigan et al., 2011; Tsipidi et al., 2017; Ma et al., 2018;
70 Lim et al., 2019; Fang et al., 2021), which is often not accounted for in many ESMs.

71 Climate models usually treat POA and SOA as non-volatile and non-reactive
72 particles that are directly emitted into the atmosphere (Kanakidou et al., 2005;
73 Tsipidi et al., 2014; Pai et al., 2020). Donahue et al. (2006) introduced the volatility
74 basis set (VBS) framework to capture the changes in OA volatility. This framework
75 describes the partitioning of OA, assuming it is semi-volatile and photochemically
76 reactive and that it is distributed across logarithmically spaced volatility bins. By
77 using this approach, both the emissions of intermediate and semi-volatile primary
78 aerosols, as well as SOA formation and its aging processes can be simulated. This
79 approach has already been implemented in several regional and global chemical
80 transport models (Tsipidi et al., 2010; Jathar et al., 2011; Shrivastava et al., 2011;
81 Bergström et al., 2012; Woody et al., 2016; Chen et al., 2019; Jiang et al., 2019) and
82 in a few ESMs (Gao et al., 2024; Irfan et al., 2024). Many of these modeling studies
83 have demonstrated improved predictions of OA concentrations by incorporating the
84 VBS framework into their simulations. However, its implementation in large-scale
85 models, such as ESMs, remains limited due to its high computational expense.

86 Tsipidi et al. (2014) developed the ORACLE module, which is based on the
87 VBS framework, and implemented it in the ECHAM/MESSy Atmospheric Chemistry
88 (EMAC) model (Jöckel et al., 2006). ORACLE reduces the computational cost by
89 utilizing a small number of surrogate OA species by employing a novel lumping
90 method. However, the 92 species used in the full configuration of the ORACLE
91 module to describe OA and its volatility are still excessive for ESM simulations
92 increasing significantly the computational cost. To address the computational
93 constraints of ESMs, Tsipidi et al. (2025) introduced a lite configuration of the
94 ORACLE module (hereafter ORACLE-lite), further reducing the number of species
95 used to describe OA and its volatility from 92 to 18. Although simplifications were
96 made to reduce the computational cost, ORACLE-lite continues to effectively
97 simulate the contributions of low volatility organic compounds (LVOCs), semi-
98 volatile organic compounds (SVOCs), IVOCs, and VOCs to SOA formation
99 (Tsipidi et al., 2025). ORACLE-lite is recommended for ESM simulations (Riipinen
100 et al., 2025).

101 The aim of this study is to incorporate a computationally efficient OA
102 volatility scheme based on ORACLE-lite into the chemistry-transport component of



103 EC-Earth3-AerChem ESM to simulate OA concentrations, composition, and
104 evolution. Section 2 provides an overview of the model, focusing mostly on the new
105 implementations. In particular, we describe the version of the EC-Earth ESM used,
106 the implemented OA volatility scheme, and the conducted simulations. In Section 3,
107 we present the model-derived OA atmospheric concentrations and their evaluation
108 with available observations. Finally, in Section 4, we discuss the impact of the VBS
109 framework on the simulated OA atmospheric concentrations and we summarize the
110 global implications of explicitly representing POA emissions in a climate–chemistry
111 model, along with the plans for future model development.

112

113 **2. Model description**

114 **2.1 The EC-Earth3 Earth System Model**

115 The EC-Earth3-AerChem configuration (EC-Earth3-AerChem version 3.5.0) of the
116 EC-Earth3 (Döscher et al., 2021) has been used for this work. EC-Earth3 contributed
117 to Phase 6 of the Coupled Model Intercomparison Project (CMIP6; Eyring et al.,
118 2016). Its atmospheric general circulation model (GCM) is based on cycle 36r4 of the
119 Integrated Forecast System (IFS), from the European Centre for Medium-Range
120 Weather Forecasts (ECMWF), which includes the H-TESSEL land surface model
121 (Balsamo et al., 2009). The ocean model is the version 3.6 of the Nucleus for
122 European Modelling of the Ocean (NEMO; Rousset et al., 2015), with sea ice
123 processes represented by the Louvain-la-Neuve sea ice model (LIM; Vancoppenolle
124 et al., 2009; Rousset et al., 2015). The majority of information exchange and
125 interpolation between modules is managed by the Ocean Atmosphere Sea Ice Soil
126 coupler, version 3 (OASIS3; Craig et al., 2017). EC-Earth3-AerChem includes TM5-
127 MP (Tracer Model 5, Massively Parallel version; Kroll et al., 2005; Huijnen et al.,
128 2010; van Noije et al., 2014; Williams et al., 2017) for the simulation of aerosols and
129 atmospheric chemistry. TM5-MP can be also used as a standalone CTM driven by
130 offline meteorological and surface fields from the ERA-Interim reanalysis, developed
131 by the European Centre for Medium-Range Weather Forecasts (ECMWF; Dee et al.,
132 2011). It simulates the atmospheric life cycle of air pollutants, including emissions,
133 advection, convection, vertical diffusion, and removal by dry and wet deposition, as
134 well as chemical and microphysical transformations. Gas-phase chemistry is
135 described by mCB05, a modified version of the CB05 carbon bond mechanism
136 (Yarwood et al., 2005; Williams et al., 2017). For the gas and particle equilibrium



137 calculations of $\text{NH}_3/\text{NH}_4^+$ and $\text{HNO}_3/\text{NO}_3^-$, the ISORROPIA-lite model is used
138 (Kakavas et al., 2022) neglecting the effect of organic aerosol water on inorganic
139 aerosol thermodynamics. The organic aerosol water contribution to the total aerosol
140 water is calculated separately, based on Myriokefalitakis et al. (2022). To simulate the
141 composition and evolution of OA the ORACLE-lite module (Tsimpidi et al., 2025) is
142 used.

143 The aerosol population and its evolution are treated by the modal two-moment
144 aerosol model M7 (Vignati et al., 2004). M7 includes four water soluble modes
145 (nucleation, Aitken, accumulation, and coarse) and three insoluble modes (Aitken,
146 accumulation, and coarse). The dry radius size ranges for the aerosol modes are
147 defined as follows: nucleation mode ($r_p < 5$ nm), Aitken mode ($5 < r_p < 50$ nm),
148 accumulation mode ($50 < r_p < 500$ nm), and coarse mode ($r_p > 500$ nm). Particles within
149 each mode are assumed to be internally mixed. Each mode follows a lognormal size
150 distribution with a fixed geometric standard deviation. The M7 model tracks the
151 evolution of both total particle number and the mass of each species within each
152 mode. In this work, we incorporated both POA and SOA into the default soluble POA
153 modes (Aitken, accumulation, and coarse) of the M7 model to track aerosol number
154 distribution. The existing M7 species also include SOA formed from biogenic VOCs
155 (Bergman et al., 2022), along with sulfate, black carbon, sea salt and dust.
156 Additionally, TM5-MP simulates the concentrations of nitrate, ammonium, and
157 methane sulfonic acid using a bulk aerosol approach. More details about TM5-MP
158 and EC-Earth3-AerChem can be found in van Noije et al. (2021) and Myriokefalitakis
159 et al. (2022).

160

161 2.2 The ORACLE module

162 ORACLE (v1.0) uses fixed, logarithmically spaced saturation concentration
163 bins and assumes bulk equilibrium between the gas and particle phases. The OA mass
164 is then distributed among the size modes (Aitken soluble, accumulation soluble, and
165 coarse soluble) following Pandis et al. (1993), using the dry radius of each size mode
166 from the M7 model. ORACLE simulates: (i) the partitioning of POA from LVOC
167 emissions, (ii) the partitioning of POA from SVOC emissions and gas-phase oxidation
168 of the remaining vapors, followed by their condensation into the particle phase to
169 form SOA, and (iii) the gas-phase oxidation of IVOC and VOC emissions and the
170 subsequent condensation of the oxidation products to form SOA. The volatility bins



171 are defined by saturation concentration (C^*) ranges of 10^{-2} to 10^{-1} $\mu\text{g m}^{-3}$ for LVOCs,
172 10^0 to 10^2 $\mu\text{g m}^{-3}$ for SVOCs, 10^3 to 10^6 $\mu\text{g m}^{-3}$ for IVOCs, and $>10^6$ $\mu\text{g m}^{-3}$ for
173 VOCs.

174 To further reduce computational expense, we implemented a lite configuration
175 of the ORACLE module (hereafter ORACLE-lite) in the TM5-MP model, which
176 represents the chemistry-transport component of the EC-Earth3-AerChem ESM by
177 introducing a reduced set of surrogate species. This includes POA and primary
178 organic gas (POG) for LVOC emissions, POA and POG for SVOC emissions, and
179 POG for IVOC emissions, as well as SOA and secondary organic gas (SOG) formed
180 through the oxidation of SVOC and IVOC emissions by hydroxyl radicals. Note
181 however, that the SOA formation from biogenic VOC emissions (isoprene and
182 monoterpenes) is already represented in the models, as described by Bergman et al.
183 (2022), while SOA formation from anthropogenic VOC emissions is neglected. As a
184 result, the number of surrogate species used to represent OA and its volatility in
185 ORACLE-lite was reduced from 18 to 9. An overview of the characteristics of the lite
186 configuration of the ORACLE module used in this study is shown in Table 1.

187

188 **2.3 Simulations**

189 In this study, present-day simulations were performed using atmosphere-only runs of
190 EC-Earth3-AerChem (hereafter referred to as EC-Earth) for the years 2000-2010. In
191 addition, standalone simulations with TM5-MP for the year 2005 driven by ERA-
192 Interim (Dee et al., 2011) were performed. In the EC-Earth simulation, TM5-MP is
193 coupled to the IFS atmospheric dynamics. Sea surface temperature and sea ice
194 concentration fields were prescribed using input files provided through the AMIP
195 interface (Taylor et al., 2000). Consequently, the atmospheric and chemistry modules
196 follow the standard EC-Earth3-AerChem configuration used in CMIP6. The IFS
197 component is configured with a horizontal resolution of T255 (approximately 80 km),
198 91 vertical levels extending up to 0.01 hPa, and a time step of 45 minutes. TM5-MP,
199 in both its standalone and EC-Earth configurations, uses a horizontal resolution of
200 $3^\circ \times 2^\circ$ (longitude \times latitude) and 34 vertical levels extending up to 0.1 hPa (~ 60 km).

201 For this work, two types of simulations were performed for both TM5-MP and
202 EC-Earth: (a) using the default OA representation and emissions, in which OA is
203 treated as non-volatile, non-reactive and emitted exclusively as POA, and (b)



204 incorporating the ORACLE-lite module with modified emissions (hereafter referred
205 to as VBS).

206 In the VBS configuration, the emission factors used to distribute traditional
207 POA emissions into LVOCs and SVOCs are based on the work of Tsimpidi et al.
208 (2025). For fossil fuel combustion sources, emission factors of 0.09 and 0.71 are
209 assigned to LVOCs and SVOCs, respectively. For biomass burning, the
210 corresponding factors are 0.2 for LVOCs and 0.5 for SVOCs. These emissions are
211 assigned to volatility bins with C^* of $10^{-2} \mu\text{g m}^{-3}$ and $10^1 \mu\text{g m}^{-3}$ for LVOCs and
212 SVOCs, respectively (Table 1). Please note that IVOCs exist almost exclusively in the
213 gas-phase (Pandis et al., 2013) and are not fully accounted for in traditional emission
214 inventories, despite their potentially substantial role in SOA formation. Previous
215 studies estimate IVOCs emissions to range from 0.25 to 2.8 times those of traditional
216 POA emissions (Schauer et al., 2002). In this study, we assume that IVOCs emissions
217 are equal to 0.3 times the traditional POA emissions for biomass burning and 1.7
218 times for fossil fuel combustion sources, following the estimates of Tsimpidi et al.
219 (2025). These emissions are assigned to the volatility bin with $C^* = 10^4 \mu\text{g m}^{-3}$.
220 Overall, LVOCs and SVOCs are assumed to be initially emitted in the particle phase
221 as POA, while IVOCs are emitted solely in the gas-phase.

222

223 **2.4 Observations**

224 To evaluate the impact of the VBS scheme on simulated aerosol concentrations, we
225 compared the models results with monthly surface-level observations of $\text{PM}_{2.5}$ OA
226 concentrations during 2005. We used data from two freely available observational
227 networks: the United States Interagency Monitoring of Protected Visual
228 Environments (IMPROVE; <https://views.cira.colostate.edu/fed/QueryWizard>, last
229 access: 2 June 2025) and the European Monitoring and Evaluation Project (EMEP;
230 <https://ebas-data.nilu.no/Default.aspx>, last access: 2 June 2025). For the IMPROVE
231 network, we used monthly OA concentrations from 174 stations while for EMEP, data
232 were available from only 3 stations for the simulated period. Please note that both
233 IMPROVE and EMEP networks measure particulate organic carbon (OC) instead of
234 total organic mass in the particles. To convert OC to organic mass, we applied a
235 constant factor. For the IMPROVE network, the suggested factor equals to 1.8
236 (Pitchford et al., 2007). For EMEP, we followed the IMPROVE network



237 recommendation and assumed a factor of 1.8 for EMEP stations to maintain
238 consistency.

239

240 2.5 Models performance

241 To evaluate the models performance, specific statistical metrics were calculated for
242 both configurations of TM5-MP and EC-Earth simulations. These include mean bias
243 (MB), mean absolute gross error (MAGE), normalized mean bias (NMB), normalized
244 mean error (NME), and root-mean-square error (RMSE) defined as follows:

$$245 MB = \frac{1}{N} \sum_{i=1}^N (P_i - O_i) \quad (1)$$

$$246 MAGE = \frac{1}{N} \sum_{i=1}^N |P_i - O_i| \quad (2)$$

$$247 NMB = \frac{\sum_{i=1}^N (P_i - O_i)}{\sum_{i=1}^N O_i} \quad (3)$$

$$248 NME = \frac{\sum_{i=1}^N |P_i - O_i|}{\sum_{i=1}^N O_i} \quad (4)$$

$$249 RMSE = \left[\frac{1}{N} \sum_{i=1}^N (P_i - O_i)^2 \right]^{1/2} \quad (5)$$

250 where P_i is the predicted OA concentration, O_i is the observed OA value at the same
251 monthly averaged time, and N is the total number of measurements used for the
252 comparison.

253 NME (in %) and MAGE (in $\mu\text{g m}^{-3}$) measure the total difference between
254 model predictions and observations, including both bias and scatter. In contrast, NMB
255 (in %) and MB (in $\mu\text{g m}^{-3}$) specifically reflect systematic errors. RMSE (in $\mu\text{g m}^{-3}$)
256 combines both the variability (scatter) and bias of the predictions into a single metric.
257 Because NME and MAGE include bias effects, their values are typically equal to or
258 greater than those of NMB and MB. When NME and NMB (or MAGE and MB) are
259 similar in magnitude, most of the error is due to bias. However, if NME and MAGE
260 are substantially larger than NMB and MB, this indicates that scatter also contributes
261 significantly to the discrepancy between predictions and observations.

262

263

264



260 **2.6 Emissions**

261 The annual present-day emissions used in the chemistry transport component of EC-
262 Earth (TM5-MP) with the VBS configuration are shown in Fig. 1. In the default OA
263 configuration, particulate organic matter is emitted exclusively as POA (Fig. S1; 52.4
264 Tg yr^{-1}) and is assumed to have constant carbon content, expressed as the ratio of
265 total OA mass to the mass of the carbon it contains. This ratio is used to convert POA
266 emissions, typically expressed as organic carbon (OC) mass to OA mass. In this
267 study, a ratio of 1.6 is applied across all POA sources based on previous works
268 (Turpin and Lim, 2001; Reid et al., 2005; Aiken et al., 2008; van Noije et al., 2021).
269 In the VBS configuration, emissions are distributed into three volatility bins based on
270 the emission factors described in Section 2: LVOCs (7.6 Tg yr^{-1}), SVOCs (31.8 Tg
271 yr^{-1}), and IVOCs (53.1 Tg yr^{-1}) (see also Table 2). LVOCs and SVOCs represent
272 POA emissions, which are lower in total than in the default OA configuration because
273 a portion of the traditional organic mass emissions is reassigned to IVOCs. The
274 corresponding annual mean emissions used for the EC-Earth simulation are shown in
275 Fig. 2. The emissions are higher in regions such as China, India, Bangladesh, southern
276 Africa, and South America. Emissions from shipping are also present over oceanic
277 regions.

278

279 **3. Results**

280 **3.1 Budget calculations**

281 This section presents the global budgets, atmospheric burdens, and lifetimes of
282 OA components from EC-Earth and standalone TM5-MP simulations during 2005
283 using the VBS configuration (Table 1). For completeness, SOA from biogenic VOCs
284 (bSOA-v) is also included.

285 In the standalone TM5-MP simulation for 2005, SOA production from SVOCs
286 (SOA-sv) and IVOCs (SOA-iv) is 19.83 Tg yr^{-1} and 37.02 Tg yr^{-1} , respectively. The
287 total annual SOA production is 109.19 Tg yr^{-1} . This value falls within the range of
288 50–380 Tg yr^{-1} of Spracklen et al. (2011) and is close to their best estimate of 140 Tg
289 yr^{-1} . The relative contributions to the annual SOA production are 18.2% from
290 SVOCs, 33.9% from IVOCs, and 47.9% from biogenic VOCs. Anthropogenic SOA
291 production is higher near source regions (Fig. 3), with hotspots in South America,
292 southern Africa, India, Bangladesh, and China. Seasonally, the production of SOA-sv
293 is higher in summer (Fig. S2), whereas SOA-iv production peaks in winter, especially



294 over India, China, and Central Africa (Fig. S3). This seasonal trend will be discussed
295 further in the next section.

296 In the EC-Earth simulation, the annual mean production for 2000-2010 of
297 SOA-sv and SOA-iv is 19.62 ± 1.67 Tg yr $^{-1}$ and 38.28 ± 7.32 Tg yr $^{-1}$, respectively
298 (Table 2; Fig. 3), with a total SOA production of 109.22 ± 10.23 Tg yr $^{-1}$. The
299 contributions to total SOA production are 18% from SVOCs, 35% from IVOCs, and
300 47% from biogenic VOCs. Annual (Fig. S4) and seasonal (Figs. S5 and S6) SOA
301 production indicate no significant differences between the TM5-MP and EC-Earth
302 simulations during 2005. Minor discrepancies arise from differences in meteorology,
303 which is predicted in EC-Earth but prescribed from reanalysis in the TM5-MP
304 simulation.

305 The contributions to the annual atmospheric burden of total OA (3.67 Tg) in
306 the standalone TM5-MP simulation are 18.7% from POA, 16.4% from SOA-sv,
307 32.9% from SOA-iv, and 32% from bSOA-v. Compared to the default simulation, in
308 which SOA is produced only from biogenic VOCs and all anthropogenic OA is
309 treated as POA, the annual atmospheric burden of total OA increased by
310 approximately 50% in the VBS simulation. In EC-Earth, the annual mean atmospheric
311 burden using the VBS configuration is 60% higher than in the default configuration,
312 reaching 3.83 ± 0.21 Tg. The respective contributions are 19.3% from POA, 15.9%
313 from SOA-sv, 34% from SOA-iv, and 30.8% from bSOA-v.

314

315 **3.2 Atmospheric concentrations**

316 The annual mean surface concentrations of POA, SOA-sv, SOA-iv, and bSOA-v in
317 the standalone TM5-MP simulation with the VBS configuration are shown in Fig. 4.
318 POA levels are higher than those of SOA-sv and SOA-iv especially in regions like
319 India and China with higher LVOC and SVOC emissions. Our simulations indicate
320 that the emitted POA undergoes evaporation and is subsequently oxidized by
321 hydroxyl radicals in the gas phase, leading to the formation of SOA-sv through re-
322 condensation. This is consistent with recent experimental studies especially for
323 biomass burning emissions (e.g., Sengupta et al., 2020; Fang et al., 2021). Biomass
324 burning emissions from residential heating are typically higher during winter, and the
325 lower temperatures enhance partitioning to the particle phase, leading to increased



326 POA concentrations, especially in regions such as China, Bangladesh, Central Africa
327 and India (Fig. S7).

328 The annual mean concentrations of SOA-sv are lower than those of POA, as
329 only a fraction of POA evaporates, undergoes photooxidation, and subsequently
330 condenses into the particle phase. The oxidation of IVOCs, producing lower-volatility
331 products, also contributes to SOA-sv formation. Please note that in ORACLE-lite, the
332 volatility bin representing SOA-sv corresponds to a C^* value of $10^{-2} \mu\text{g m}^{-3}$,
333 indicating low volatility and a predominant presence in the particle phase. The higher
334 SOA-sv concentrations predicted during summer compared to winter (Table S1; Fig.
335 S8) are due to the higher summer temperatures promoting POA evaporation, and the
336 increased sunlight which enhances subsequent photooxidation and formation of SOA.

337 Higher annual mean concentrations of SOA-iv compared to SOA-sv are
338 predicted, primarily due to the higher emissions of IVOCs (Table 1; Fig. 1) and the
339 different formation mechanism. IVOCs can directly undergo oxidation by hydroxyl
340 radicals, producing lower-volatility products that subsequently condense into the
341 particle phase. Predicted SOA-iv concentrations are higher in winter than in summer
342 (Table S1), particularly in regions such as China, India, Bangladesh, and Europe (Fig.
343 S9). This is attributed to increased biomass burning emissions in these regions and
344 lower temperatures, which enhance partitioning of the semi-volatile OA components
345 into the particle phase. However, in regions such as South America and southern
346 Africa, where major rainforests like the Amazon and Congo Basin are located, SOA-
347 iv concentrations are higher during summer due to wildfires.

348 The annual mean surface concentrations of total OA in the standalone TM5-
349 MP simulation with the VBS configuration are shown in Fig. 5. Higher concentrations
350 are predicted in regions with higher precursor emissions, while as altitude increases
351 the concentrations of OA decrease as expected, with higher concentrations between
352 15°S and 45°N (Fig. 5b). At higher altitudes, SOA concentrations are higher
353 compared to POA, because organic gases can be efficiently transported upward and
354 oxidized, leading to the formation of lower-volatility SOA (Fig. S10). Additionally,
355 SOA formed at these altitudes tends to have a longer atmospheric lifetime, as it is less
356 affected by wet and dry deposition processes (Tsimpidi et al., 2014).

357 The VBS configuration predicts significantly higher annual mean total OA
358 concentrations (by up to 100%) compared to the default TM5-MP configuration,
359 particularly in regions such as India, China, and northern Africa (Fig. 5c). Significant



360 increases are also predicted over oceanic regions, including the Indian, Atlantic and
361 Pacific Oceans. In addition to S/IVOC emissions from shipping (Fig. 1), this increase
362 is largely driven by the long-range transport of IVOCs, which contributes to SOA-iv
363 formation far from emission sources (Aiken et al., 2009; Hildebrandt et al., 2010).
364 This is further supported by the higher increases in total OA concentrations predicted
365 in these regions during winter compared to summer (Fig. S11), attributed to higher
366 SOA-iv levels in the colder season (Fig. S9). At higher altitudes, the VBS
367 configuration in general predicts higher OA concentrations than the default
368 configuration, particularly between 0° and 45°N (Fig. 5d). However, in the uppermost
369 levels of the model, the default configuration predicts higher OA concentrations.
370 Nevertheless, in both simulations, these values are extremely low (below 0.001 μg
371 m^{-3}), rendering the absolute differences negligible.

372 The annual mean surface concentrations of POA and SOA in the EC-Earth
373 simulation with the VBS configuration for 2000-2010 are shown in Fig. 6. Similar to
374 the TM5-MP simulation, higher SOA concentrations than POA are predicted. With
375 increasing altitude, SOA concentrations remain higher than POA because organic
376 gases are efficiently transported upward and oxidized, producing lower-volatility
377 SOA. However, compared to the TM5-MP simulation, there are some differences in
378 the global distribution of the annual mean surface total OA for 2005 (Fig. S12). More
379 specifically, in regions such as South America, Africa, India, and China, EC-Earth
380 predicts higher total OA concentrations (up to 4 $\mu\text{g m}^{-3}$) during 2005 due to the higher
381 production of SOA-iv. There are also regions such as Europe in which TM5-MP
382 predicts higher total OA concentrations than EC-Earth. At higher altitudes, TM5-MP
383 in general predicts higher OA concentrations than EC-Earth, except in the region
384 between 5° S and 10°N up to 600 hPa (Fig. S12). However, in all cases, the
385 differences are lower than 0.5 $\mu\text{g m}^{-3}$. These discrepancies stem from differences in
386 meteorology since EC-Earth uses meteorology predicted by IFS, while TM5-MP
387 relies on prescribed reanalysis data. More specifically, in these regions, either lower
388 predicted temperatures or lower precipitation rates in EC-Earth affect OA
389 concentrations through partitioning and deposition, respectively (Fig. S13).

390 Overall, higher concentrations of OA are predicted by both models in regions
391 such as India, South America, southern Africa, and China, where precursor emission
392 levels are higher. The annual global mean surface concentration of total OA in the
393 TM5-MP simulation using the VBS configuration is 1.07 $\mu\text{g m}^{-3}$, corresponding to an



394 increase of 25% relative to the default configuration. In EC-Earth, the corresponding
395 annual global mean surface concentration is $1.16 \mu\text{g m}^{-3}$, representing an increase of
396 30% relative to the default configuration. The contributions of individual OA
397 components to the annual global mean surface concentration of OA are 29.9% from
398 POA, 13.1% from SOA-sv, 29% from biogenic SOA, and 28% from SOA-iv. This
399 highlights the substantial role of IVOCs in contributing to total OA, despite their
400 omission from traditional emission inventories. Additionally, our simulations indicate
401 that temperature influences the partitioning of oxidized IVOCS into the
402 particle phase, with lower temperatures favoring this process. In contrast, oxidized
403 SVOC products are treated as low-volatility compounds in the ORACLE-lite module
404 and predominantly remain in the particle phase under typical atmospheric conditions.

405

406 **3.3 Models evaluation**

407 Figure 7 shows the comparison between predicted $\text{PM}_{2.5}$ OA concentrations and
408 corresponding measurements for both of TM5-MP and EC-Earth simulations during
409 2005. Each point on the scatterplot represents a monthly average value at a specific
410 monitoring station. Compared to the default configuration, the VBS configuration of
411 TM5-MP predicts higher OA concentrations at all stations, with model results
412 generally falling closer to the 1:1 line. More specifically, in both TM5-MP
413 simulations, OA concentrations are generally underpredicted at the examined stations,
414 as indicated by negative MB and NMB values (Table 3). However, the VBS
415 configuration reduces this underprediction by approximately half ($\text{MB} = -0.28 \mu\text{g}$
416 m^{-3} , $\text{NMB} = -13.2\%$) compared to the default configuration ($\text{MB} = -0.57 \mu\text{g m}^{-3}$,
417 $\text{NMB} = -27.1\%$). Additionally, both NME and RMSE values, which are relatively
418 low in the default simulation ($\text{NME} = 42\%$, $\text{RMSE} = 1.57 \mu\text{g m}^{-3}$), improve further in
419 the VBS simulation ($\text{NME} = 38.9\%$, $\text{RMSE} = 1.5 \mu\text{g m}^{-3}$), indicating reduced scatter.
420 The same applies for MAGE, which decreased from $0.89 \mu\text{g m}^{-3}$ in the default
421 simulation to $0.82 \mu\text{g m}^{-3}$ in the VBS simulation. The corresponding EC-Earth
422 metrics for 2005 for both configurations are also shown in Table 3. EC-Earth also
423 underpredicts OA concentrations at the examined stations. However, the VBS
424 configuration of EC-Earth reduces the underprediction by approximately a factor of
425 three ($\text{MB} = -0.17 \mu\text{g m}^{-3}$, $\text{NMB} = -8.1\%$) compared to the default configuration
426 ($\text{MB} = -0.54 \mu\text{g m}^{-3}$, $\text{NMB} = -25.7\%$). Compared to the standalone TM5-MP



427 simulation with the VBS configuration, MB and NMB are lower, whereas MAGE and
428 NME are higher (MAGE = $0.94 \mu\text{g m}^{-3}$, NME = 44.5%). This mainly indicates that
429 the additional SOA-iv production in EC-Earth, resulting from differences in
430 meteorological treatment, further reduces systematic errors but increases bias and
431 scatter.

432 Figure 8 shows the annual cycle of monthly mean $\text{PM}_{2.5}$ OA concentrations at
433 EMEP and IMPROVE sites in the TM5-MP offline and EC-Earth simulations during
434 2005. For TM5-MP, the VBS configuration predicts higher concentrations throughout
435 the year compared to the default configuration. However, $\text{PM}_{2.5}$ OA is still
436 underpredicted, particularly at European sites and during winter. This underestimation
437 may result from the omission of oxidation of biomass burning emissions by NO_3
438 radicals, as well as uncertainties in the biomass burning emissions (Reddington et al.,
439 2019; Hua et al., 2024). The same applies for EC-Earth simulations.

440 Despite uncertainties in the emissions for fuel combustion and biomass
441 burning, the predictions of OA concentrations using the VBS configuration show
442 improved performance and are generally in good agreement with measurements.
443 Please note that the formation of SOA from anthropogenic VOC emissions (to reduce
444 computational cost) and from oxidation by NO_3 radicals is neglected in the model,
445 which may partially explain the remaining bias. The previous study of Tsimpidi et al.
446 (2014) indicated that SOA from anthropogenic VOCs contributes only about 15% to
447 the global average surface OA concentration. Additionally, the absence of biogenic
448 SOA formation in the models from sesquiterpenes may also contribute to the
449 underprediction (Bergman et al., 2022; Dada et al., 2023).

450

451 **4. Summary and conclusions**

452 We have implemented a lite configuration of the ORACLE module into the TM5-MP
453 CTM, which represents the chemistry-transport component of the EC-Earth3-
454 AerChem ESM. This version of the module applies the VBS framework to simulate
455 SOA formation from LVOCs, SVOCs, and IVOCs.

456 The incorporation of ORACLE-lite significantly improved the representation
457 of OA formation and atmospheric behavior both in the standalone TM5-MP and the
458 EC-Earth. The models evaluation against monthly measured $\text{PM}_{2.5}$ OA concentrations
459 from Europe (EMEP) and US (IMPROVE) stations indicated that OA concentrations
460 were generally underpredicted. However, the VBS configuration reduced NMB by



461 nearly half in TM5-MP and a factor of three in EC-Earth and improved the overall
462 agreement. There is a remaining NMB in both models (-13% in TM5-MP and -8% in
463 EC-Earth) which can be explained by the absence of SOA formation from
464 anthropogenic VOC emissions and sesquiterpenes or via oxidation by NO_3 radicals,
465 which can be subjects for future work. Compared to the traditional POA (default)
466 configuration, the VBS implementation increased the global annual mean surface OA
467 concentration in TM5-MP by 25% to $1.07 \mu\text{g m}^{-3}$ and the atmospheric OA burden by
468 50%, to 3.67 Tg. Corresponding predictions from EC-Earth were slightly higher, with
469 a surface OA concentration of $1.16 \mu\text{g m}^{-3}$ and an atmospheric burden of 3.83 Tg,
470 representing increases of 30% and 60%, respectively. These changes resulted
471 primarily from the inclusion of SOA production from S/IVOCs and the treatment of
472 gas-particle partitioning and chemical aging, processes absent in the default OA
473 scheme.

474 Our results indicate that SOA is the dominant contributor to total OA surface
475 concentrations and atmospheric burden, whereas POA contributes less than 30% to
476 both, highlighting the importance of including gas-phase oxidation and partitioning of
477 OA in ESMs. The seasonal and spatial variability of SOA was also better captured,
478 with higher concentrations predicted in regions with intense biomass burning and
479 anthropogenic activity, such as India, China, and sub-Saharan Africa.

480 Overall, the lite configuration of ORACLE module captures well the key
481 processes driving OA formation and evolution, offering a more realistic simulation of
482 OA concentrations without significantly increasing computational cost
483 (approximately 8%). This efficient and robust configuration supports future studies on
484 the climatic impacts of OA within ESMs.

485

486 **Acknowledgments**

487 This work was supported by the REINFORCE research project, implemented in the
488 framework of HFRI called “Basic Research Financing (Horizontal Support of all
489 Sciences)” under the National Recovery and Resilience Plan “Greece 2.0” funded by
490 the European Union - Next Generation EU (HFRI project no. 15155). We also
491 acknowledge support by the project Atmospheric nanoparticles, air quality and human
492 health (NANOSOMs) funded by the Hellenic Foundation for Research and Innovation
493 (HFRI) (grant no. 11504). Computational time was granted from the National



494 Infrastructures for Research and Technology S.A. (GRNET S.A.) in the National HPC
495 facility – ARIS – under project ID 010003 (AEROSIM). Acknowledgement is made
496 for the use of ECMWF's computing and archive facilities in this research (Special
497 Project: EC-Earth Atmospheric Composition developments).

498

499 **Code availability**

500 The EC-Earth3-AerChem code (version 3.5.0) is available to members of the EC-
501 Earth consortium via the EC-Earth development portal (<https://dev.ec-earth.org/>, last
502 accessed: 12 November 2025). Model components developed at ECMWF, such as the
503 IFS atmospheric model, are the intellectual property of ECMWF and its member
504 states. Access to the EC-Earth3-AerChem version 3.5.0 source code can be requested
505 through the EC-Earth website (<http://www.ec-earth.org/>, last accessed: 12 November
506 2025) and may be granted upon signing a software license agreement with ECMWF.
507 Due to licensing restrictions, access is currently limited to European users. The TM5-
508 MP version 1.2 code with modifications for the VBS framework of this work can be
509 found at Zenodo (<https://doi.org/10.5281/zenodo.18254761>). The lite configuration of
510 the ORACLE v1.0 code, which is part of the ECHAM/MESSy Atmospheric
511 Chemistry (EMAC) model, can be obtained by applying for an EMAC license, or
512 upon request by emailing A. Tsimpidi (a.tsimpidi@fz-juelich.de). More information
513 can be found on the MESSy Consortium website (<http://www.messy-interface.org>).
514 ISORROPIA-lite is available upon request at <https://isorropia.epfl.ch>. Post-processing
515 scripts used for creating the main figures of the manuscript are available at Zenodo
516 (<https://doi.org/10.5281/zenodo.18255310>).

517

518 **Data availability**

519 The data used for the model evaluation in Figs. 7 and 8 are from two freely available
520 observational networks: the United States Interagency Monitoring of Protected Visual
521 Environments (IMPROVE; <https://views.cira.colostate.edu/fed/QueryWizard/>, last
522 access: 2 June 2025) for fine organic mass in the IMPROVE Aerosol dataset and the
523 European Monitoring and Evaluation Project (EMEP; <https://ebas-data.nilu.no/Default.aspx>, last access: 2 June 2025) for PM_{2.5} organic carbon in the EMEP
524 framework. The data produced in the study are available from the authors upon
525 request.

527



528 **Competing interests**

529 The authors declare that they have no conflicts of interest.

530

531 **Author contributions**

532 SK contributed to the implementation of the ORACLE-lite module into the model,
533 conducted the CTM simulations, analyzed the results, and wrote the paper. SM
534 designed the study, integrated the ORACLE-lite code into the model, conducted the
535 ESM simulations, and also contributed to writing the paper. APT and VAK provided
536 the ORACLE-lite code, supported its integration into the model, and contributed to
537 manuscript preparation. SNP supervised the study and contributed to manuscript
538 writing.

539

540 **References**

541 Aiken, A. C., DeCarlo, P. F., Kroll, J. H., Worsnop, D. R., Huffman, J. A., Docherty,
542 K. S., Ulbrich, I. M., Mohr, C., Kimmel, J. R., Sueper, D., Sun, Y., Zhang, Q.,
543 Trimborn, A., Northway, M., Ziemann, P. J., Canagaratna, M. R., Onasch, T.
544 B., Alfarra, M. R., Prevot, A. S. H., Dommen, J., Duplissy, J., Metzger, A.,
545 Baltensperger, U., and Jimenez, J. L.: O/C and OM/OC ratios of primary,
546 secondary, and ambient organic aerosols with high-resolution time-of-flight
547 aerosol mass spectrometry, *Environ. Sci. Technol.*, 42, 4478–4485, doi:
548 10.1021/es703009q, 2008.

549 Aiken, A. C., Salcedo, D., Cubison, M. J., Huffman, J. A., DeCarlo, P. F., Ulbrich, I.
550 M., Docherty, K. S., Sueper, D., Kimmel, J. R., Worsnop, D. R., Trimborn, A.,
551 Northway, M., Stone, E. A., Schauer, J. J., Volkamer, R. M., Fortner, E., de
552 Foy, B., Wang, J., Laskin, A., Shutthanandan, V., Zheng, J., Zhang, R.,
553 Gaffney, J., Marley, N. A., Paredes-Miranda, G., Arnott, W. P., Molina, L. T.,
554 Sosa, G., and Jimenez, J. L.: Mexico City aerosol analysis during MILAGRO
555 using high resolution aerosol mass spectrometry at the urban supersite (T0) –
556 Part 1: Fine particle composition and organic source apportionment, *Atmos.
557 Chem. Phys.*, 9, 6633–6653, doi:10.5194/acp-9-6633-2009, 2009.

558 Balsamo, G., Viterbo, P., Beijars, A., van den Hurk, B., Hirschi, M., Betts, A. K.,
559 and Scipal, K.: A revised hydrology for the ECMWF model: Verification from
560 field site to terrestrial water storage and impact in the integrated forecast
561 system, *J. Hydrometeorol.*, 10, 623–643, doi: 10.1175/2008JHM1068.1, 2009.



562 Bergman, T., Makkonen, R., Schrödner, R., Swietlicki, E., Phillips, V. T. J., Le Sager,
563 P., and van Noije, T.: Description and evaluation of a secondary organic
564 aerosol and new particle formation scheme within TM5-MP v1.2, *Geosci.
565 Model Dev.*, 15, 683–713, doi:10.5194/gmd-15-683-2022, 2022.

566 Bergström, R., Denier van der Gon, H. A. C., Prévôt, A. S. H., Yttri, K. E., and
567 Simpson, D.: Modelling of organic aerosols over Europe (2002–2007) using a
568 volatility basis set (VBS) framework: application of different assumptions
569 regarding the formation of secondary organic aerosol, *Atmos. Chem. Phys.*,
570 12, 8499–8527, doi: 10.5194/acp-12-8499-2012, 2012.

571 Bougiatioti, A., Nikolaou, P., Stavroulas, I., Kouvarakis, G., Weber, R., Nenes, A.,
572 Kanakidou, M., and Mihalopoulos, N.: Particle water and pH in the eastern
573 Mediterranean: source variability and implications for nutrient availability,
574 *Atmos. Chem. Phys.*, 16, 4579–4591, doi: 10.5194/acp-16-4579-2016, 2016.

575 Chen, X., Yang, W., Wang, Z., Li, J., Hu, M., An, J., Wu, Q., Wang, Z., Chen, H.,
576 and Wei, Y.: Improving new particle formation simulation by coupling a
577 volatility-basis set (VBS) organic aerosol module in NAQPMS+APM, *Atmos.
578 Environ.*, 204, 1–11, doi: 10.1016/j.atmosenv.2019.01.053, 2019.

579 Craig, A., Valcke, S., and Coquart, L.: Development and performance of a new
580 version of the OASIS coupler, *OASIS3-MCT_3.0*, *Geosci. Model Dev.*, 10,
581 3297–3308, doi: 10.5194/gmd-10-3297-2017, 2017.

582 Crippa, M., Canonaco, F., Slowik, J. G., El Haddad, I., DeCarlo, P. F., Mohr, C.,
583 Heringa, M. F., Chirico, R., Marchand, N., Temime-Roussel, B., Abidi, E.,
584 Poulain, L., Wiedensohler, A., Baltensperger, U., and Prévôt, A. S. H.:
585 Primary and secondary organic aerosol origin by combined gas-particle phase
586 source apportionment, *Atmos. Chem. Phys.*, 13, 8411–8426, doi: 10.5194/acp-
587 13-8411-2013, 2013.

588 Dada, L., Stolzenburg, D., Simon, M., Fischer, L., Heinritzi, M., Wang, M., Xiao, M.,
589 Vogel, A. L., Ahonen, L., Amorim, A., Baalbaki, R., Baccarini, A.,
590 Baltensperger, U., Bianchi, F., Daellenbach, K. R., DeVivo, J., Dias, A.,
591 Dommen, J., Duplissy, J., Finkenzeller, H., Hansel, A., He, X-C.,
592 Hofbauer, V., Hoyle, C. R., Kangasluoma, J., Kim, C., Kürten, A.,
593 Kvashnin, A., Mauldin, R., Makhmutov, V., Marten, R., Mentler, B., Nie, W.,
594 Petäjä, T., Quéléver, L. L. J., Saathoff, H., Tauber, C., Tome, A., Molteni, U.,
595 Volkamer, R., Wagner, R., Wagner, A. C., Wimmer, D., Winkler, P. M.,



596 Yan, C., Zha, Q., Rissanen, M., Gordon, H., Curtius, J., Worsnop, D. R.,
597 Lehtipalo, K., Donahue, N. M., Kirkby, J., El Haddad, I., and Kulmala, M.:
598 Role of sesquiterpenes in biogenic new particle formation, *Sci. Adv.*, 9, 36,
599 doi:10.1126/sciadv.adi5297, 2023.

600 Dee, D. P., Uppala, S. M., Simmons, A. J., Berrisford, P., Poli, P., Kobayashi, S.,
601 Andrae, U., Balmaseda, M. A., Balsamo, G., Bauer, P., Bechtold, P., Beljaars,
602 A. C. M., van de Berg, L., Bidlot, J., Bormann, N., Delsol, C., Dragani, R.,
603 Fuentes, M., Geer, A. J., Haimberger, L., Healy, S. B., Hersbach, H., Hólm,
604 E. V., Isaksen, L., Kållberg, P., Köhler, M., Matricardi, M., McNally, A. P.,
605 Monge-Sanz, B. M., Morcrette, J.-J., Park, B.-K., Peubey, C., de Rosnay, P.,
606 Tavolato, C., Thépaut, J.-N., and Vitart, F.: The ERA-Interim reanalysis:
607 configuration and performance of the data assimilation system, *Q. J. Roy.
608 Meteor. Soc.*, 137, 553–597, doi: 10.1002/qj.828, 2011.

609 Donahue, N. M., Robinson, A. L., Stanier, C. O., and Pandis, S. N.: Coupled
610 partitioning, dilution, and chemical aging of semivolatile organics, *Environ.
611 Sci. Technol.*, 40, 2635–2643, 2006.

612 Döscher, R., Acosta, M., Alessandri, A., Anthoni, P., Arsouze, T., Bergman, T.,
613 Bernardello, R., Boussetta, S., Caron, L.-P., Carver, G., Castrillo, M.,
614 Catalano, F., Cvijanovic, I., Davini, P., Dekker, E., Doblas-Reyes, F. J.,
615 Docquier, D., Echevarria, P., Fladrich, U., Fuentes-Franco, R., Gröger, M., v.
616 Hardenberg, J., Hieronymus, J., Karami, M. P., Keskinen, J.-P., Koenigk, T.,
617 Makkonen, R., Massonnet, F., Ménégoz, M., Miller, P. A., Moreno-Chamarro,
618 E., Nieradzik, L., van Noije, T., Nolan, P., O'Donnell, D., Ollinaho, P., van
619 den Oord, G., Ortega, P., Prims, O. T., Ramos, A., Reerink, T., Rousset, C.,
620 Ruprich-Robert, Y., Le Sager, P., Schmitt, T., Schrödner, R., Serva, F.,
621 Sicardi, V., Sloth Madsen, M., Smith, B., Tian, T., Tourigny, E., Uotila, P.,
622 Vancoppenolle, M., Wang, S., Wårllind, D., Willén, U., Wyser, K., Yang, S.,
623 Yepes-Arbós, X., and Zhang, Q.: The EC-Earth3 Earth system model for the
624 Coupled Model Intercomparison Project 6, *Geosci. Model Dev.*, 15, 2973–
625 3020, doi: 10.5194/gmd-15-2973-2022, 2022.

626 Eyring, V., Bony, S., Meehl, G. A., Senior, C. A., Stevens, B., Stouffer, R. J., and
627 Taylor, K. E.: Overview of the Coupled Model Intercomparison Project Phase
6 (CMIP6) experimental design and organization, *Geosci. Model Dev.*, 9,
628 1937–1958, doi:10.5194/gmd-9-1937-2016, 2016.



630 Fang, Z., Li, C., He, Q., Czech, H., Gröger, T., Zeng, J., Fang, H., Xiao, S., Pardo, M.,
631 Hartner, E., Meidan, D., Wang, X., Zimmermann, R., Laskin, A., and Rudich,
632 Y.: Secondary organic aerosols produced from photochemical oxidation of
633 secondarily evaporated biomass burning organic gases: Chemical composition,
634 toxicity, optical properties, and climate effect, *Environ. Int.*, 157, 106801, doi:
635 10.1016/j.envint.2021.106801, 2021.

636 Gao, C. Y., Bauer, S. E., Tsigaridis, K., and Im, U.: Global influence of organic
637 aerosol volatility on aerosol microphysical processes: Composition and
638 number, *Journal of Advances in Modeling Earth Systems*, 16,
639 e2023MS004185, doi: 10.1029/2023MS004185, 2024.

640 Grieshop, A. P., Logue, J. M., Donahue, N. M., and Robinson, A. L.: Laboratory
641 investigation of photochemical oxidation of organic aerosol from wood fires 1:
642 measurement and simulation of organic aerosol evolution, *Atmos. Chem.
643 Phys.*, 9, 1263–1277, doi: 10.5194/acp-9-1263-2009, 2009.

644 Heald, C. L., Jacob, D. J., Park, R. J., Russell, L. M., Huebert, B. J., Seinfeld, J. H.,
645 Liao, H., and Weber, R. J.: A large organic aerosol source in the free
646 troposphere missing from current models, *Geophys. Res. Lett.*, 32, L18809,
647 doi: 10.1029/2005gl023831, 2005.

648 Hennigan, C. J., Miracolo, M. A., Engelhart, G. J., May, A. A., Presto, A. A., Lee, T.,
649 Sullivan, A. P., McMeeking, G. R., Coe, H., Wold, C. E., Hao, W.-M.,
650 Gilman, J. B., Kuster, W. C., de Gouw, J., Schichtel, B. A., Collett Jr., J. L.,
651 Kreidenweis, S. M., and Robinson, A. L.: Chemical and physical
652 transformations of organic aerosol from the photo-oxidation of open biomass
653 burning emissions in an environmental chamber, *Atmos. Chem. Phys.*, 11,
654 7669–7686, doi:10.5194/acp-11-7669-2011, 2011.

655 Hildebrandt, L., Engelhart, G. J., Mohr, C., Kostenidou, E., Lanz, V. A., Bougiatioti,
656 A., DeCarlo, P. F., Prevot, A. S. H., Baltensperger, U., Mihalopoulos, N.,
657 Donahue, N. M., and Pandis, S. N.: Aged organic aerosol in the Eastern
658 Mediterranean: the Finokalia Aerosol Measurement Experiment – 2008,
659 *Atmos. Chem. Phys.*, 10, 4167–4186, doi:10.5194/acp-10-4167-2010, 2010.

660 Hu, W., Hu, M., Hu, W., Jimenez, J. L., Yuan, B., Chen, W., Wang, M., Wu, Y.,
661 Chen, C., Wang, Z., Peng, J., Zeng, L., and Shao, M.: Chemical composition,
662 sources and aging process of sub-micron aerosols in Beijing: contrast between



663 summer and winter, *J. Geophys. Res.-Atmos.*, 121, 1955–1977, doi:
664 10.1002/2015JD024020, 2016.

665 Hua, W., Lou, S., Huang, X., Xue, L., Ding, K., Wang, Z., and Ding, A.: Diagnosing
666 uncertainties in global biomass burning emission inventories and their impact
667 on modeled air pollutants, *Atmos. Chem. Phys.*, 24, 6787–6807, doi:
668 10.5194/acp-24-6787-2024, 2024.

669 Huijnen, V., Williams, J., van Weele, M., van Noije, T., Krol, M., Dentener, F.,
670 Segers, A., Houweling, S., Peters, W., de Laat, J., Boersma, F., Bergamaschi,
671 P., van Velthoven, P., Le Sager, P., Eskes, H., Alkemade, F., Scheele, R.,
672 Nédélec, P., and Pätz, H.-W.: The global chemistry transport model TM5:
673 description and evaluation of the tropospheric chemistry version 3.0, *Geosci.
674 Model Dev.*, 3, 445–473, doi: 10.5194/gmd-3-445-2010, 2010.

675 IPCC: Climate Change 2021: The Physical Science Basis. Working Group I
676 Contribution to the Sixth Assessment Report of the Intergovernmental Panel
677 on Climate Change, edited by: Masson-Delmotte, V., Zhai, P., Pirani, A.,
678 Connors, S. L., Péan, C., Berger, S., Caud, N., Chen, Y., Goldfarb, L., Gomis,
679 M. I., Huang, M., Leitzell, K., Lonnoy, E., Matthews, J. B. R., Maycock, T.
680 K., Waterfield, T., Yelekçi, O., Yu, R., and Zhou, B., Cambridge University
681 Press, Cambridge, United Kingdom and New York, NY, USA,
682 doi:10.1017/9781009157896.2391 pp., 2021.

683 Irfan, M., Kühn, T., Yli-Juuti, T., Laakso, A., Holopainen, E., Worsnop, D. R.,
684 Virtanen, A., and Kokkola, H.: A model study investigating the sensitivity of
685 aerosol forcing to the volatilities of semi-volatile organic compounds, *Atmos.
686 Chem. Phys.*, 24, 8489–8506, doi: 10.5194/acp-24-8489-2024, 2024.

687 Jathar, S. H., Farina, S. C., Robinson, A. L., and Adams, P. J.: The influence of semi-
688 volatile and reactive primary emissions on the abundance and properties of
689 global organic aerosol, *Atmos. Chem. Phys.*, 11, 7727–7746, doi:10.5194/acp-
690 11-7727- 2011, 2011.

691 Jiang, J., Aksoyoglu, S., El-Haddad, I., Ciarelli, G., Denier van der Gon, H. A. C.,
692 Canonaco, F., Gilardoni, S., Paglione, M., Minguillón, M. C., Favez, O.,
693 Zhang, Y., Marchand, N., Hao, L., Virtanen, A., Florou, K., O'Dowd, C.,
694 Ovadnevaite, J., Baltensperger, U., and Prévôt, A. S. H.: Sources of organic
695 aerosols in Europe: a modeling study using CAMx with modified volatility



696 basis set scheme, *Atmos. Chem. Phys.*, 19, 15247–15270, doi: 10.5194/acp-
697 19-15247-2019, 2019.

698 Jöckel, P., Tost, H., Pozzer, A., Brühl, C., Buchholz, J., Ganzeveld, L., Hoor, P.,
699 Kerkweg, A., Lawrence, M. G., Sander, R., Steil, B., Stiller, G., Tanarhte, M.,
700 Taraborrelli, D., van Aardenne, J., and Lelieveld, J.: The atmospheric
701 chemistry general circulation model ECHAM5/MESSy1: consistent
702 simulation of ozone from the surface to the mesosphere, *Atmos. Chem. Phys.*,
703 6, 5067– 5104, doi:10.5194/acp-6-5067-2006, 2006.

704 Kakavas, S., Pandis, S. N., and Nenes, A.: ISORROPIA-lite: A comprehensive
705 atmospheric aerosol thermodynamics module for Earth System Models, *Tellus*
706 B, 74, 1–23, 2022.

707 Kanakidou, M., Seinfeld, J. H., Pandis, S. N., Barnes, I., Dentener, F. J., Facchini, M.
708 C., Van Dingenen, R., Ervens, B., Nenes, A., Nielsen, C. J., Swietlicki, E.,
709 Putaud, J. P., Balkanski, Y., Fuzzi, S., Horth, J., Moortgat, G. K.,
710 Winterhalter, R., Myhre, C. E. L., Tsigaridis, K., Vignati, E., Stephanou, E.
711 G., and Wilson, J.: Organic aerosol and global climate modelling: a review,
712 *Atmos. Chem. Phys.*, 5, 1053–1123, doi: 10.5194/acp-5-1053-2005, 2005.

713 Krol, M., Houweling, S., Bregman, B., van den Broek, M., Segers, A., van Velthoven,
714 P., Peters, W., Dentener, F., and Bergamaschi, P.: The two-way nested global
715 chemistry-transport zoom model TM5: algorithm and applications, *Atmos.*
716 *Chem. Phys.*, 5, 417–432, doi: 10.5194/acp-5-417-2005, 2005.

717 Kroll, J. H. and Seinfeld, J. H.: Chemistry of secondary organic aerosol: Formation
718 and evolution of low-volatility organics in the atmosphere, *Atmos. Environ.*,
719 42, 3593–3624, 2008.

720 Lim, C. Y., Hagan, D. H., Coggon, M. M., Koss, A. R., Sekimoto, K., de Gouw, J.,
721 Warneke, C., Cappa, C. D., and Kroll, J. H.: Secondary organic aerosol
722 formation from the laboratory oxidation of biomass burning emissions, *Atmos.*
723 *Chem. Phys.*, 19, 12797–12809, doi: 10.5194/acp-19-12797-2019, 2019.

724 Ma, P., Zhang, P., Shu, J., Yang, B., and Zhang, H.: Characterization of secondary
725 organic aerosol from photo-oxidation of gasoline exhaust and specific sources
726 of major components, *Environ. Pollut.*, 232, 65–72, doi:
727 10.1016/j.envpol.2017.09.018, 2018.

728 Monks, P., Granier, C., Fuzzi, S., Stohl, A., Williams, M., Akimoto, H., Amann, M.,
729 Baklanov, A., Baltensperger, U., Bey, I., Blake, N., Blake, R., Carslaw, K.,



730 Cooper, O., Dentener, F., Fowler, D., Fragkou, E., Frost, G., Generoso, S.,
731 Ginoux, P., Grewe, V., Guenther, A., Hansson, H., Henne, S., Hjorth, J.,
732 Hofzumahaus, A., Huntrieser, H., Isaksen, I., Jenkin, M., Kaiser, J.,
733 Kanakidou, M., Klimont, Z., Kulmala, M., Laj, P., Lawrence, M., Lee, J.,
734 Liousse, C., Maione, M., McFiggans, G., Metzger, A., Mieville, A.,
735 Moussiopoulos, N., Orlando, J., O'Dowd, C., Palmer, P., Parrish, D., Petzold,
736 A., Platt, U., Pöschl, U., Prévôt, A., Reeves, C., Reimann, S., Rudich, Y.,
737 Sellegri, K., Steinbrecher, R., Simpson, D., ten Brink, H., Theloke, J., van der
738 Werf, G., Vautard, R., Vestreng, V., Vlachokostas, C., and von Glasow, R.:
739 Atmospheric composition change – global and regional air quality, *Atmos.*
740 *Environ.*, 43, 5268–5350, doi: 10.1016/j.atmosenv.2009.08.021, 2009.

741 Myriokefalitakis, S., Bergas-Massó, E., Gonçalves-Ageitos, M., Pérez García-Pando,
742 C., van Noije, T., Le Sager, P., Ito, A., Athanasopoulou, E., Nenes, A.,
743 Kanakidou, M., Krol, M. C., and Gerasopoulos, E.: Multiphase processes in
744 the EC-Earth model and their relevance to the atmospheric oxalate, sulfate,
745 and iron cycles, *Geosci. Model Dev.*, 15, 3079–3120, doi: 10.5194/gmd-15-
746 3079-2022, 2022.

747 Nault, B. A., Campuzano-Jost, P., Day, D. A., Schroder, J. C., Anderson, B.,
748 Beyersdorf, A. J., Blake, D. R., Brune, W. H., Choi, Y., Corr, C. A., de Gouw,
749 J. A., Dibb, J., DiGangi, J. P., Diskin, G. S., Fried, A., Huey, L. G., Kim, M.
750 J., Knote, C. J., Lamb, K. D., Lee, T., Park, T., Pusede, S. E., Scheuer, E.,
751 Thornhill, K. L., Woo, J.-H., and Jimenez, J. L.: Secondary organic aerosol
752 production from local emissions dominates the organic aerosol budget over
753 Seoul, South Korea, during KORUS-AQ, *Atmos. Chem. Phys.*, 18, 17769–
754 17800, doi: 10.5194/acp-18-17769-2018, 2018.

755 Pai, S. J., Heald, C. L., Pierce, J. R., Farina, S. C., Marais, E. A., Jimenez, J. L.,
756 Campuzano-Jost, P., Nault, B. A., Middlebrook, A. M., Coe, H., Shilling, J.
757 E., Bahreini, R., Dingle, J. H., and Vu, K.: An evaluation of global organic
758 aerosol schemes using airborne observations, *Atmos. Chem. Phys.*, 20, 2637–
759 2665, doi: 10.5194/acp-20-2637-2020, 2020.

760 Pandis, S. N., Wexler, A. S., and Seinfeld, J. H.: Secondary organic aerosol formation
761 and transport. 2. Predicting the ambient secondary organic aerosol-size
762 distribution, *Atmos. Environ. AGen.*, 27, 2403–2416, 1993.



763 Pandis, S. N., Donahue, N. M., Murphy, B. N., Riipinen, I., Fountoukis, C., Karnezi,
764 E., Patoulas, D., and Skyllakou, K.: Introductory lecture: atmospheric organic
765 aerosols: insights from the combination of measurements and chemical
766 transport models, Faraday Discussion, 165, 9–24, doi: 10.1039/c3fd00108c,
767 2013.

768 Pitchford, M., Malm, W., Schichtel, B., Kumar, N., Lowenthal, D., and Hand, J.:
769 Revised Algorithm for Estimating Light Extinction from IMPROVE Particle
770 Speciation Data, J. Air Waste Manage., 57, 1326–1336, doi: 10.3155/1047-
771 3289.57.11.1326, 2007.

772 Reddington, C. L., Morgan, W. T., Derbyshire, E., Brito, J., Coe, H., Artaxo, P.,
773 Scott, C. E., Marsham, J., and Spracklen, D. V.: Biomass burning aerosol over
774 the Amazon: analysis of aircraft, surface and satellite observations using a
775 global aerosol model, Atmos. Chem. Phys., 19, 9125–9152, doi: 10.5194/acp-
776 19-9125-2019, 2019.

777 Reid, J. S., Koppmann, R., Eck, T. F., and Eleuterio, D. P.: A review of biomass
778 burning emissions part II: intensive physical properties of biomass burning
779 particles, Atmos. Chem. Phys., 5, 799–825, doi: 10.5194/acp-5-799-2005,
780 2005.

781 Riipinen, I., Talvinen, S., Chassaing, A., Georgakaki P., Li, X., García-Pando, P. C.,
782 Bergman, T., Kommula, M. S., Proske, U., Gkouvousis, A., Tsimpidi, P. A.,
783 Chatziparaschos, M., Neuberger, A., Karydis, A. V., Calderón, M. S.,
784 Romakkaniemi, S., Partridge, G. D., Khadir, T., Dada, L., van Noije, T.,
785 Decesari, S., Seland, Ø., Zieger, P., Bender, F., Carlslaw, K., Cermak, J.,
786 Costa-Surós, M., Ageitos, M. G., Gramlich, Y., Haugvaldstad, W. O.,
787 Holopainen, E., Hoose, C., Jorba, O., Kakavas, S., Kanakidou, M., Kokkola, H.,
788 Krehci, R., Kühn, T., Kulmala, M., La Sager, P., Makkonen, R., Manavi, E. I. S.,
789 Mentel, F. T., Milousis, A., Myriokefalitakis, S., Nenes, A., Nieminen, T., Pandis, S. N.,
790 Patoulas, D., Petäjä, T., Quaas, J., Regayre, L., Scholz, M. C. S., Schulz, M., Skyllakou, K.,
791 Sousse, R., Stier, P., Thomas, M. A., Villinger, J. T., Virtanen, A., Wyser, K., and Ekman, M. L. A.: Treatment
792 of Key Aerosol and Cloud Processes in Earth System Models –
793 Recommendations from the FORCeS Project, Tellus B, under revision, 2025.

794 Robinson, A. L., Donahue, N. M., Shrivastava, M. K., Weitkamp, E. A., Sage, A. M.,
795 Grieshop, A. P., Lane, T. E., Pierce, J. R., and Pandis, S. N.: Rethinking



797 organic aerosols: Semivolatile emissions and photochemical aging, *Science*,
798 315, 1259–1262, 2007.

799 Rousset, C., Vancoppenolle, M., Madec, G., Fichefet, T., Flavoni, S., Barthélemy, A.,
800 Benshila, R., Chanut, J., Levy, C., Masson, S., and Vivier, F.: The Louvain-
801 La-Neuve sea ice model LIM3.6: global and regional capabilities, *Geosci.
802 Model Dev.*, 8, 2991–3005, doi: 10.5194/gmd-8-2991-2015, 2015.

803 Schauer, J. J., Kleeman, M. J., Cass, G. R., and Simoneit, B. R. T.: Measurement of
804 emissions from air pollution sources. 5. C₁-C₃₂ organic compounds from
805 gasoline-powered motor vehicles, *Environ Sci Technol*, 36, 1169–1180, doi:
806 10.1021/es0108077, 2002.

807 Sengupta, D., Samburova, V., Bhattarai, C., Watts, A. C., Moosmüller, H., and
808 Khlystov, A. Y.: Polar semivolatile organic compounds in biomass-burning
809 emissions and their chemical transformations during aging in an oxidation
810 flow reactor, *Atmos. Chem. Phys.*, 20, 8227–8250, doi: 10.5194/acp-20-8227-
811 2020, 2020.

812 Shrivastava, M., Fast, J., Easter, R., Gustafson Jr., W. I., Zaveri, R. A., Jimenez, J. L.,
813 Saide, P., and Hodzic, A.: Modeling organic aerosols in a megacity: comparison of simple and complex representations of the volatility basis set
814 approach, *Atmos. Chem. Phys.*, 11, 6639–6662, doi: 10.5194/acp-11-6639-
815 2011, 2011.

816 Shrivastava, M., Cappa, C. D., Fan, J., Goldstein, A. H., Guenther, A. B.,
817 Jimenez, J. L., Kuang, C., Laskin, A., Martin, S. T., Ng, N. L., Petaja, T.,
818 Pierce, J. R., Rasch, P. J., Roldin, P., Seinfeld, J. H., Shilling, J., Smith, J. N.,
819 Thornton, J. A., Volkamer, R., Wang, J., Worsnop, D. R., Zaveri, R. A.,
820 Zelenyuk, A., and Zhang, Q.: Recent advances in understanding secondary
821 organic aerosol: implications for global climate forcing, *Rev. Geophys.*, 55,
822 509–559, doi: 10.1002/2016RG000540, 2017.

823 Spracklen, D. V., Jimenez, J. L., Carslaw, K. S., Worsnop, D. R., Evans, M. J., Mann,
824 G. W., Zhang, Q., Canagaratna, M. R., Allan, J., Coe, H., McFiggans, G., Rap,
825 A., and Forster, P.: Aerosol mass spectrometer constraint on the global
826 secondary organic aerosol budget, *Atmos. Chem. Phys.*, 11, 12109–12136,
827 doi: 10.5194/acp-11-12109-2011, 2011.

828 Taylor, K. E., Williamson, D., and Zwiers, F.: The sea surface temperature and sea ice
829 concentration boundary conditions for AMIP II simulations, *Progr. Clim.*
830



831 Model Diagnosis Intercomp., PCMDI Report No. 60, 1–24
832 , <https://pcmdi.llnl.gov/report/pdf/60.pdf?id=42> (last access: 14 May 2025),
833 2000.

834 Tsigaridis, K., Daskalakis, N., Kanakidou, M., Adams, P. J., Artaxo, P., Bahadur, R.,
835 Balkanski, Y., Bauer, S. E., Bellouin, N., Benedetti, A., Bergman, T.,
836 Berntsen, T. K., Beukes, J. P., Bian, H., Carslaw, K. S., Chin, M., Curci, G.,
837 Diehl, T., Easter, R. C., Ghan, S. J., Gong, S. L., Hodzic, A., Hoyle, C. R.,
838 Iversen, T., Jathar, S., Jimenez, J. L., Kaiser, J. W., Kirkevåg, A., Koch, D.,
839 Kokkola, H., Lee, Y. H., Lin, G., Liu, X., Luo, G., Ma, X., Mann, G. W.,
840 Mihalopoulos, N., Morcrette, J.-J., Müller, J.-F., Myhre, G., Myriokefalitakis,
841 S., Ng, N. L., O'Donnell, D., Penner, J. E., Pozzoli, L., Pringle, K. J., Russell,
842 L. M., Schulz, M., Sciare, J., Seland, Ø., Shindell, D. T., Sillman, S., Skeie, R.
843 B., Spracklen, D., Stavrakou, T., Steenrod, S. D., Takemura, T., Tiitta, P.,
844 Tilmes, S., Tost, H., van Noije, T., van Zyl, P. G., von Salzen, K., Yu, F.,
845 Wang, Z., Wang, Z., Zaveri, R. A., Zhang, H., Zhang, K., Zhang, Q., and
846 Zhang, X.: The AeroCom evaluation and intercomparison of organic aerosol
847 in global models, *Atmos. Chem. Phys.*, 14, 10845–10895, doi: 10.5194/acp-
848 14-10845-2014, 2014.

849 Tsimpidi, A. P., Karydis, V. A., Zavala, M., Lei, W., Molina, L., Ulbrich, I. M.,
850 Jimenez, J. L., and Pandis, S. N.: Evaluation of the volatility basis-set
851 approach for the simulation of organic aerosol formation in the Mexico City
852 metropolitan area, *Atmos. Chem. Phys.*, 10, 525–546, doi:10.5194/acp-10-
853 525-2010, 2010.

854 Tsimpidi, A. P., Karydis, V. A., Pozzer, A., Pandis, S. N., and Lelieveld, J.: ORACLE
855 (v1.0): module to simulate the organic aerosol composition and evolution in
856 the atmosphere, *Geosci. Model Dev.*, 7, 3153–3172, doi: 10.5194/gmd-7-
857 3153-2014, 2014.

858 Tsimpidi, A. P., Karydis, V. A., Pandis, S. N., and Lelieveld, J.: Global combustion
859 sources of organic aerosols: model comparison with 84 AMS factor-analysis
860 data sets, *Atmos. Chem. Phys.*, 16, 8939–8962, doi: 10.5194/acp-16-8939-
861 2016, 2016.

862 Tsimpidi, A. P., Karydis, V. A., Pandis, S. N., and Lelieveld, J.: Global-scale
863 combustion sources of organic aerosols: sensitivity to formation and removal



864 mechanisms, *Atmos. Chem. Phys.*, 17, 7345–7364, doi: 10.5194/acp-17-7345-
865 2017, 2017.

866 Tsimpidi, A. P., Scholz, S. M. C., Milousis, A., Mihalopoulos, N., and Karydis, V. A.:
867 Aerosol composition trends during 2000–2020: in-depth insights from model
868 predictions and multiple worldwide near-surface observation datasets, *Atmos.*
869 *Chem. Phys.*, 25, 10183–10213, doi: 10.5194/acp-25-10183-2025, 2025.

870 Turpin, B. J. and Lim, H.-J.: Species contributions to PM_{2.5} mass concentrations:
871 Revisiting common assumptions for estimating organic mass, *Aerosol Sci.*
872 *Technol.*, 35, 602–610, doi: 10.1080/02786820119445, 2001.

873 Vancoppenolle, M., Fichefet, T., Goosse, H., Bouillon, S., Madec, G., and Maqueda,
874 M. A. M.: Simulating the mass balance and salinity of Arctic and Antarctic sea
875 ice. 1. Model description and validation, *Ocean Model.*, 27, 33–53, doi:
876 10.1016/j.ocemod.2008.10.005, 2009.

877 van Noije, T., Le Sager, P., Segers, A. J., van Velthoven, P. F. J., Krol, M. C.,
878 Hazeleger, W., Williams, A. G., and Chambers, S. D.: Simulation of
879 tropospheric chemistry and aerosols with the climate model EC-Earth, *Geosci.*
880 *Model Dev.*, 7, 2435–2475, doi: 10.5194/gmd-7-2435-2014, 2014.

881 van Noije, T., Bergman, T., Le Sager, P., O'Donnell, D., Makkonen, R., Gonçalves-
882 Ageitos, M., Döscher, R., Fladrich, U., von Hardenberg, J., Keskinen, J.-P.,
883 Korhonen, H., Laakso, A., Myriokefalitakis, S., Ollinaho, P., Pérez García-
884 Pando, C., Reerink, T., Schrödner, R., Wyser, K., and Yang, S.: EC-Earth3-
885 AerChem: a global climate model with interactive aerosols and atmospheric
886 chemistry participating in CMIP6, *Geosci. Model Dev.*, 14, 5637–5668, doi:
887 10.5194/gmd-14-5637-2021, 2021.

888 Vignati, E., Wilson, J., and Stier, P.: M7: An efficient size-resolved aerosol
889 microphysics module for large-scale aerosol transport models, *J. Geophys.*
890 *Res.*, 109, D22202, doi: 10.1029/2003JD004485, 2004.

891 Williams, J. E., Boersma, K. F., Le Sager, P., and Verstraeten, W. W.: The high-
892 resolution version of TM5-MP for optimized satellite retrievals: description
893 and validation, *Geosci. Model Dev.*, 10, 721–750, doi: 10.5194/gmd-10-721-
894 2017, 2017.

895 Woody, M. C., Baker, K. R., Hayes, P. L., Jimenez, J. L., Koo, B., and Pye, H. O. T.:
896 Understanding sources of organic aerosol during CalNex-2010 using the



897 CMAQ-VBS, *Atmos. Chem. Phys.*, 16, 4081–4100, doi: 10.5194/acp-16-
898 4081-2016, 2016.

899 Yarwood, G., Rao, S., Yocke, M., and Whitten, G. Z.: Updates to the Carbon Bond
900 Chemical Mechanism: CB05, Research Triangle
901 Park, https://www.camx.com/Files/CB05_Final_Report_120805.pdf (last
902 access: April 2025), 2005.

903 Zhang, Q., Jimenez, J. L., Canagaratna, M. R., Allan, J. D., Coe, H., Ulbrich, I.,
904 Alfarra, M. R., Takami, A., Middlebrook, A. M., Sun, Y. L., Dzepina, K.,
905 Dunlea, E., Docherty, K., DeCarlo, P. F., Salcedo, D., Onasch, T., Jayne, J. T.,
906 Miyoshi, T., Shimono, A., Hatakeyama, S., Takegawa, N., Kondo, Y.,
907 Schneider, J., Drewnick, F., Borrmann, S., Weimer, S., Demerjian, K.,
908 Williams, P., Bower, K., Bahreini, R., Cottrell, L., Griffin, R. J., Rautiainen,
909 J., Sun, J. Y., Zhang, Y. M., and R., W. D.: Ubiquity and dominance of
910 oxygenated species in organic aerosols in anthropogenically-influenced
911 Northern Hemisphere midlatitudes, *Geophys. Res. Lett.*, 34, L13801, doi:
912 10.1029/2007GL029979, 2007.

913 Zhang, B.: The effect of aerosols to climate change and society, *J. Geosci. Environ.
914 Protect.*, 8, 55, doi: 10.4236/ gep.2020.88006, 2020.

915
916
917
918
919
920
921
922
923
924
925
926
927
928
929
930



931 **Table 1:** Overview of the ORACLE-lite module characteristics, including volatility
932 classification, evolution processes, and OA formation types for each emission
933 class

Emissions	C* ($\mu\text{g m}^{-3}$)	Representative volatility bin ($\mu\text{g m}^{-3}$)	Evolution in ORACLE-lite	OA type
LVOCs	10^{-2} - 10^{-1}	10^{-2}	Gas/particle partitioning	POA
SVOCs	10^0 - 10^2	10^1	Gas/particle partitioning and aging	POA and SOA
IVOCs	10^3 - 10^6	10^4	Aging and gas/particle partitioning	SOA
VOCs	$>10^6$	$>10^6$	Aging and gas/particle partitioning	SOA

934

935

936

937

938

939

940

941

942

943

944

945

946

947

948

949

950

951

952

953

954

955



956 **Table 2:** Global budgets, atmospheric burdens and lifetimes of **(a)** POA, **(b)** SOA-sv,
 957 **(c)** SOA-iv, **(d)** bSOA-v for EC-Earth during 2000-2010 and TM5-MP during
 958 2005 with the VBS configuration

	EC-Earth (2000-2010)	TM5-MP (2005)
LVOCs emissions (Tg yr ⁻¹)	7.40±3.98	7.54
SVOCs emissions (Tg yr ⁻¹)	31.42±10.89	31.81
IVOCs emissions (Tg yr ⁻¹)	52.78±9.34	53.13
(a) POA		
Evaporation (Tg yr ⁻¹)	3.57±0.35	3.81
Dry deposition (Tg yr ⁻¹)	3.48±0.79	3.26
Wet deposition (Tg yr ⁻¹)	31.70±8.52	31.58
Atmospheric burden (Tg)	0.73±0.04	0.69
Lifetime (days)	6.85	6.49
(b) SOA-sv		
Production (Tg yr ⁻¹)	19.62±1.67	19.83
Dry deposition (Tg yr ⁻¹)	2.02±0.17	1.97
Wet deposition (Tg yr ⁻¹)	17.56±2.63	17.41
Atmospheric burden (Tg)	0.60±0.03	0.60
Lifetime (days)	11.13	11.38
(c) SOA-iv		
Production (Tg yr ⁻¹)	38.28±7.32	37.02
Dry deposition (Tg yr ⁻¹)	3.90±0.57	3.37
Wet deposition (Tg yr ⁻¹)	34.26±6.39	32.39
Atmospheric burden (Tg)	1.35±0.07	1.21
Lifetime (days)	12.92	12.33
(d) bSOA-v		
Production (Tg yr ⁻¹)	51.31±1.24	52.34
Dry deposition (Tg yr ⁻¹)	0.69±0.07	0.40
Wet deposition (Tg yr ⁻¹)	50.67±6.70	50.58
Atmospheric burden (Tg)	1.15±0.06	1.18
Lifetime (days)	8.19	8.42



960 **Table 3:** Evaluation metrics comparing monthly averaged predicted PM_{2.5} OA
961 concentrations with IMPROVE and EMEP observations for the simulations of
962 TM5-MP and EC-Earth during 2005

Simulations	Number of measurements	Mean observed ($\mu\text{g m}^{-3}$)	Mean predicted ($\mu\text{g m}^{-3}$)	MB ($\mu\text{g m}^{-3}$)	MAGE ($\mu\text{g m}^{-3}$)	NMB (%)	NME (%)	RMSE ($\mu\text{g m}^{-3}$)
TM5-MP (Default)	2124	2.11	1.54	-0.57	0.89	-27.1	42.0	1.57
TM5-MP (VBS)	2124	2.11	1.83	-0.28	0.82	-13.2	38.9	1.50
EC-Earth (Default)	2124	2.11	1.57	-0.54	0.96	-25.7	45.6	1.68
EC-Earth (VBS)	2124	2.11	1.94	-0.17	0.94	-8.1	44.5	1.61

963

964

965

966

967

968

969

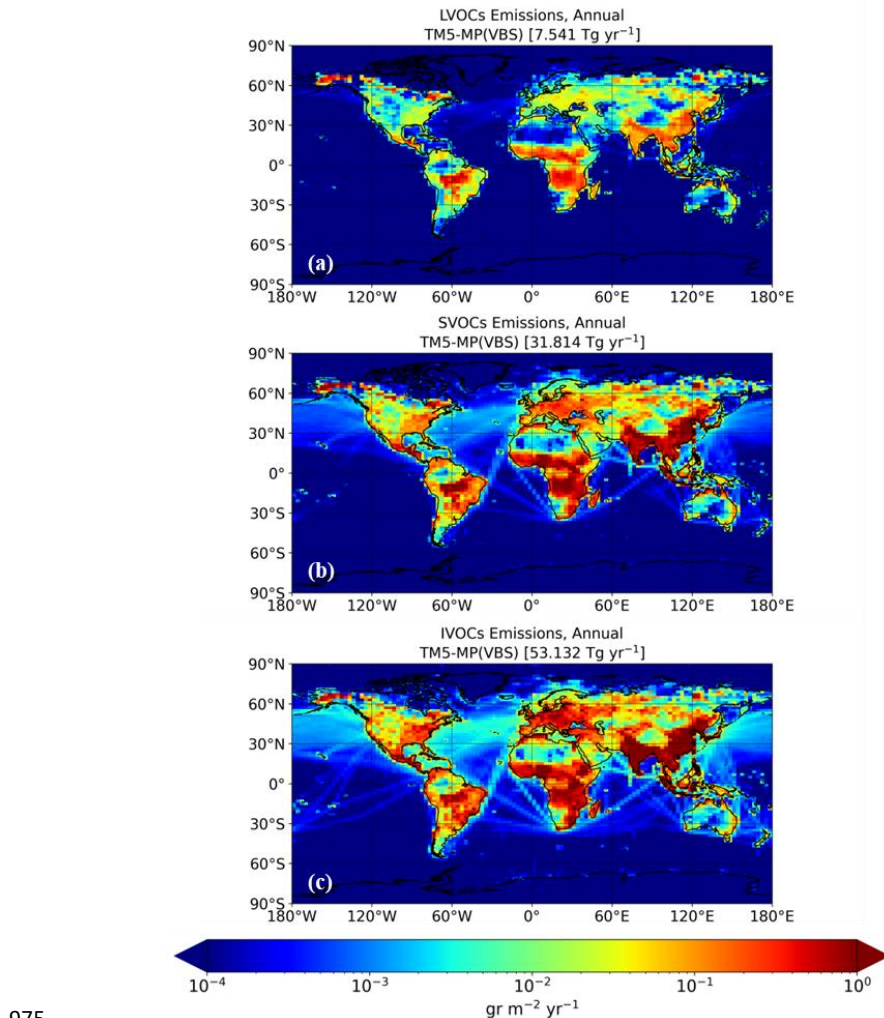
970

971

972

973

974



975

976 **Figure 1.** Annual emissions (in $\text{gr m}^{-2} \text{ yr}^{-1}$) of: (a) low volatile organic compounds
977 (LVOCs), (b) semi-volatile organic compounds (SVOCs), and (c) intermediate
978 volatile organic compounds (IVOCs) applied in the standalone TM5-MP simulation
979 during 2005.

980

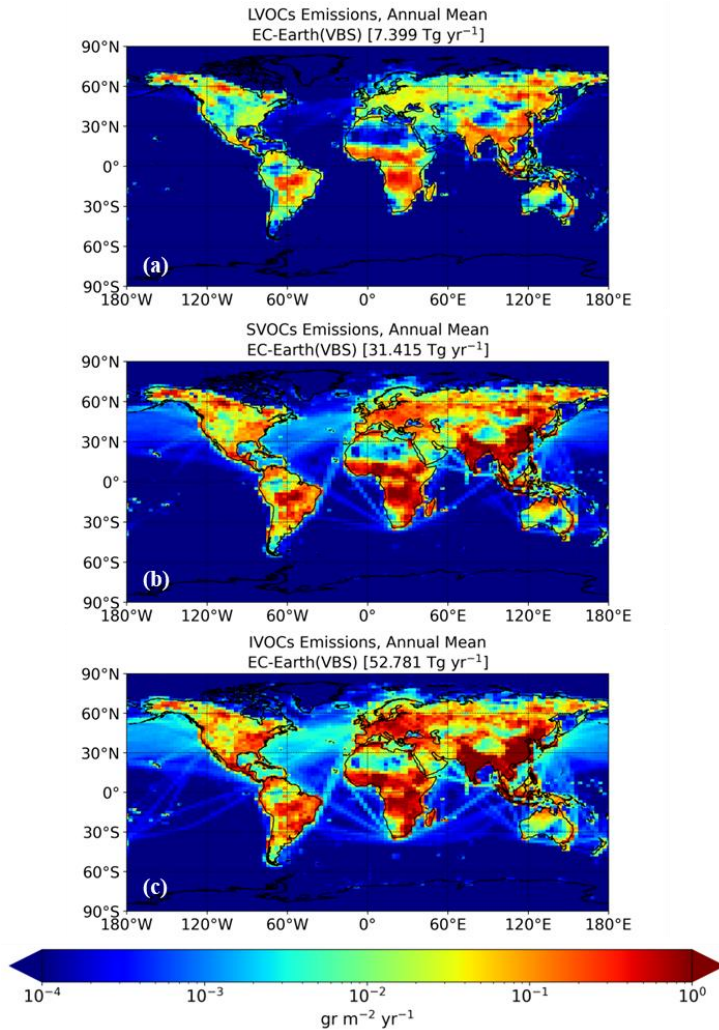
981

982

983

984

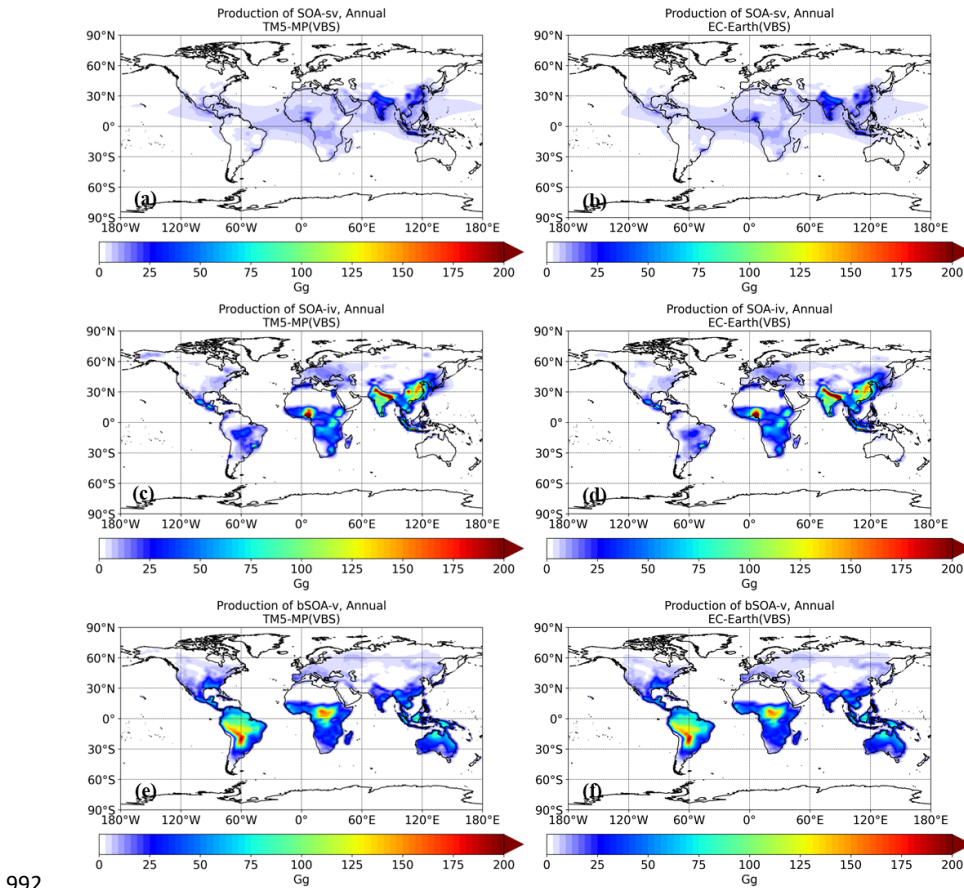
985



986

987 **Figure 2.** Annual mean emissions (in $\text{gr m}^{-2} \text{ yr}^{-1}$) of: (a) low volatile organic
988 compounds (LVOCs), (b) semi-volatile organic compounds (SVOCs), and (c)
989 intermediate volatile organic compounds (IVOCs) applied in the EC-Earth simulation
990 during 2000-2010.

991



992

993 **Figure 3.** Annual production of SOA (in Gg) as simulated using the VBS
994 configuration of TM5-MP during 2005 (left column) and the corresponding EC-Earth
995 predictions during 2000-2010 (right column) for: (a), (b) SOA-sv, and (c), (d) SOA-
996 iv. For completeness, annual SOA production from biogenic VOCs (bSOA-v) in
997 panels (e) and (f) is also shown.

998

999

1000

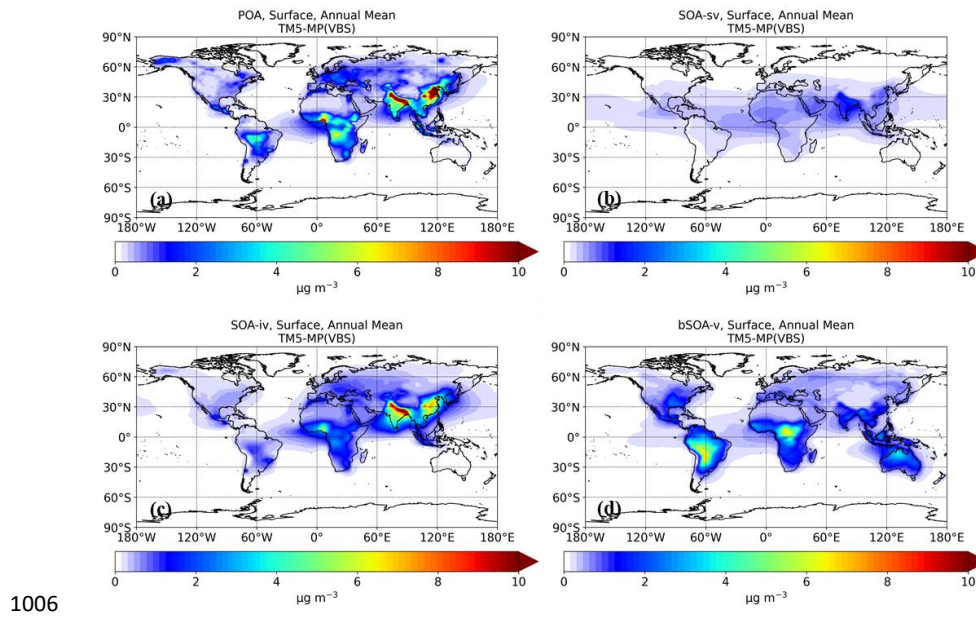
1001

1002

1003

1004

1005

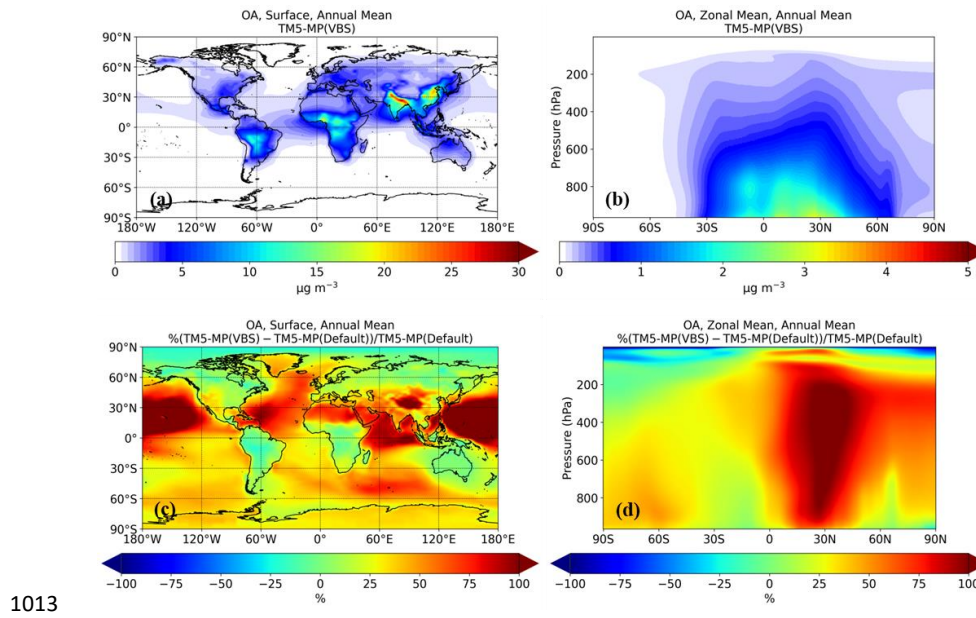


1006

1007 **Figure 4.** Annual mean surface concentrations (in $\mu\text{g m}^{-3}$) of: (a) POA, (b) SOA from
1008 SVOCs (SOA-sv), and (c) SOA from IVOCs (SOA-iv) as simulated using the VBS
1009 configuration of TM5-MP during 2005. For completeness, SOA concentrations from
1010 biogenic VOCs (bSOA-v) in panel (d) are also shown.

1011

1012



1013

1014 **Figure 5.** Annual mean concentrations of total organic aerosol (in $\mu\text{g m}^{-3}$): (a) surface
1015 concentrations, and (b) zonal values as simulated using the VBS configuration of
1016 TM5-MP during 2005. Panels (c) and (d) show the corresponding relative differences
1017 (in %) compared to the previous (default) model configuration. A positive change
1018 indicates that the VBS configuration predicts more than the default.

1019

1020

1021

1022

1023

1024

1025

1026

1027

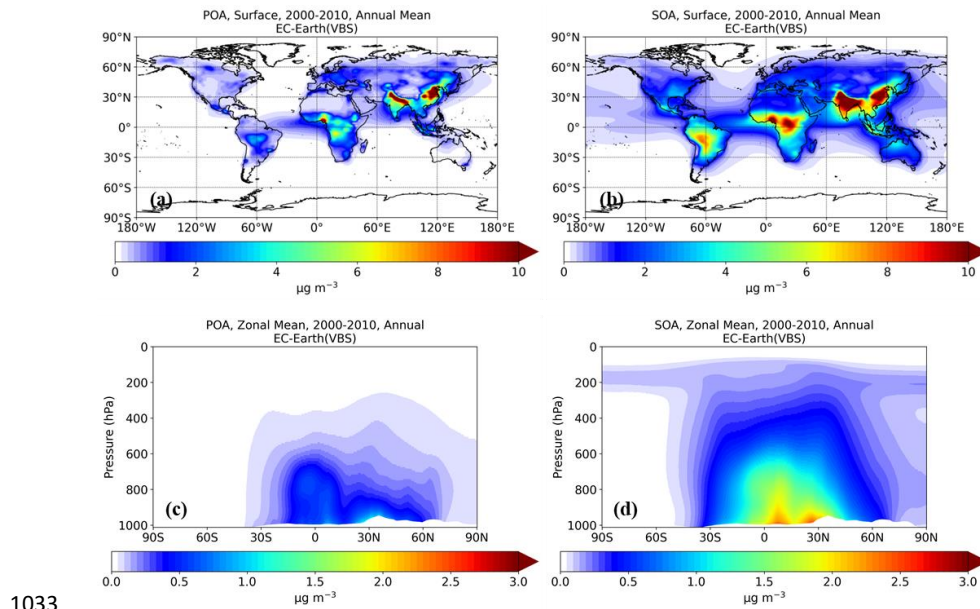
1028

1029

1030

1031

1032



1033

1034 **Figure 6.** Annual mean concentrations of POA and SOA (in $\mu\text{g m}^{-3}$): **(a), (b)** surface
1035 concentrations, and **(c), (d)** zonal values as simulated using the VBS configuration of
1036 EC-Earth during 2000-2010.

1037

1038

1039

1040

1041

1042

1043

1044

1045

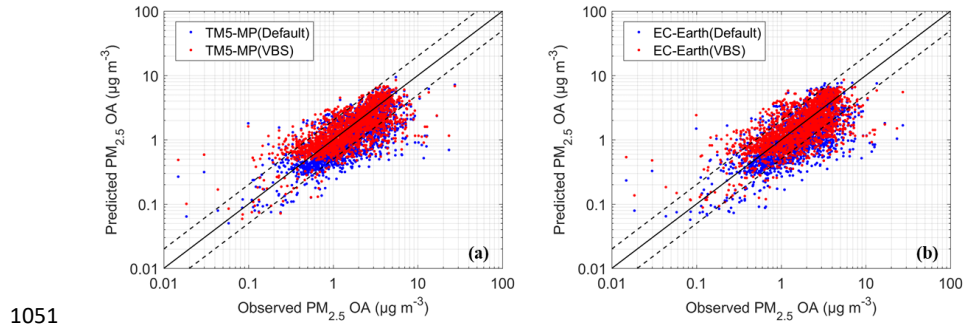
1046

1047

1048

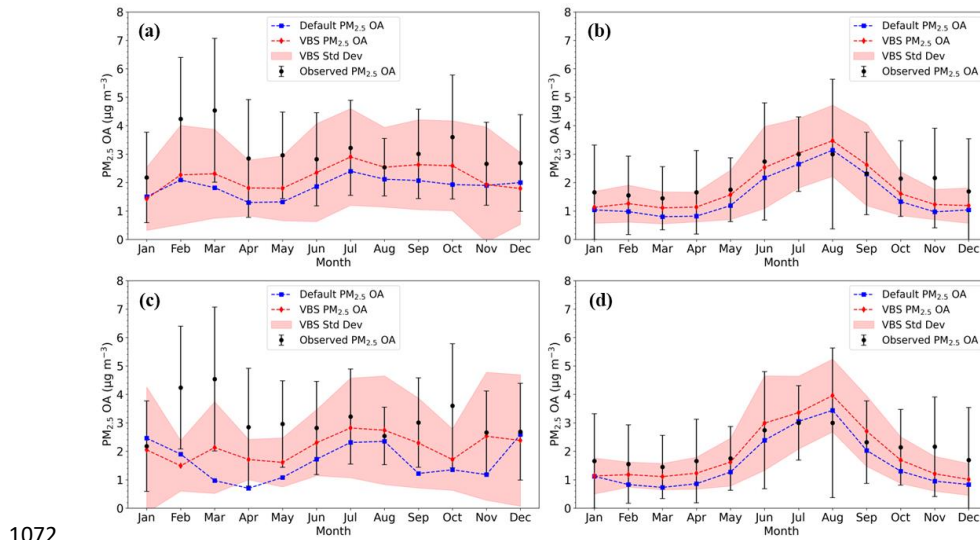
1049

1050



1051 **Figure 7.** Organic mass concentrations from simulations of: (a) TM5-MP, and (b)
1052 EC-Earth during 2005. Scatterplots compare predicted $\text{PM}_{2.5}$ OA concentrations (in
1053 $\mu\text{g m}^{-3}$) with observations from the IMPROVE and EMEP monitoring networks.
1054 Models results are shown for the default configuration (blue) and the VBS
1055 configuration (red). Each point represents a monthly average value at a monitoring
1056 site.
1057

1058
1059
1060
1061
1062
1063
1064
1065
1066
1067
1068
1069
1070
1071



1073 **Figure 8.** Annual cycles of monthly mean PM_{2.5} OA concentrations during 2005. The
1074 top row shows results from the standalone TM5-MP simulations at: **(a)** EMEP sites
1075 and **(b)** IMPROVE sites, while the bottom row shows results from the EC-Earth
1076 simulation at: **(c)** EMEP sites and **(d)** IMPROVE sites. The red line represents the
1077 mean predicted by the VBS simulation, with red shading indicating the standard
1078 deviation. The blue line represents the mean predicted by the default simulation.
1079 Black dots show the observed mean values, with vertical lines showing the
1080 corresponding standard deviations.

1081